Textured multilayered piezoelectric structures for energy conversion

Bjørnetun Haugen, Astri; Ringgaard, Erling; Levassort, Franck

Published in:
Journal of Physics: Energy

Link to article, DOI:
10.1088/2515-7655/ab5f30

Publication date:
2020

Document Version
Publisher's PDF, also known as Version of record

Textured multilayered piezoelectric structures for energy conversion

JPhys Energy

PAPER

Textured multilayered piezoelectric structures for energy conversion

Astri Bjørnetun Haugen[1,4], **Erling Ringgaard**[2] and **Franck Levassort**[3]

[1] Department of Energy Conversion and Storage, Technical University of Denmark, Fysikvej, Building 310, DK-2800 Kgs. Lyngby, Denmark
[2] Meggitt A/S, Porthusvej 4, 3490 Kvistgaard, Denmark
[3] GREMAN UMR 7347, University of Tours, CNRS, INSA CVL, 26 Rue Pierre et Marie Curie, 37100 Tours, France
[4] Author to whom any correspondence should be addressed.

E-mail: ahua@dtu.dk

Keywords: piezoelectricity, texture, ceramics, energy harvester, ultrasound

OPEN ACCESS

RECEIVED
31 October 2019

REVISED
4 December 2019

ACCEPTED FOR PUBLICATION
5 December 2019

PUBLISHED
23 December 2019

Abstract

Piezoelectric materials are essential for the conversion between mechanical and electrical energy, for example in ultrasound imaging and vibrational energy harvesting. Here, we are making and exploring the effects of a new design: co-sintered multilayers with texture (grains of a preferential crystallographic direction). The motivation is the combination of increased piezoelectric response in certain crystallographic directions; multilayer structures where thick films rather than bulk materials can allow higher frequency operation and large area; and co-sintering to avoid detrimental effects from gluing layers together. Samples of the lead-free piezoelectric material $Li_{0.06}(K_{0.52}Na_{0.48})_{0.94}Nb_{0.71}Ta_{0.29}O_3$ with 0.25 mol% Mn (KNNLTM) were made by tape casting and co-sintering. $NaNbO_3$ platelets with (100) orientation which were used as templates to introduce texture, and polymethyl methacrylate (PMMA) was used as a pore forming agent for making porous substrates. The electrical impedances of the co-sintered samples were recorded and analyzed by equivalent electrical circuit modelling. A texture up to 85% in the [100] crystallographic direction was obtained. The samples displayed ferro- and piezoelectricity, with a maximum thickness coupling coefficient ($k_t = 0.18$) between mechanical and electrical energy in the most textured sample. This demonstrates that the introduction of texture in multilayered, co-sintered piezoelectrics shows promise for improving devices for ultrasound imaging or energy harvesting.

Introduction

Energy conversion between the mechanical and the electrical domain is important in many existing, as well as upcoming technologies. Piezoelectric materials, due to their coupling between mechanical deformation and charge generation, are well suited for this purpose. Many piezoelectrics based on the perovskite-structured $Pb(Zr,Ti)O_3$ ceramics [1, 2] have been developed with high efficiency for the energy conversion [3]. Since these materials are also ferroelectric, alignment of the polarization found in each part of the polycrystalline materials is possible, causing an efficient transduction between mechanical and electrical energy: electrical surface charge in response to mechanical deformation, and strain in response to electric field. For example, in energy harvesters, the piezoelectric material can convert mechanical energy to electricity with a high energy density [3, 4], and in ultrasound transducers, the rapid generation of ultrasound waves and the conversion of back-reflected waves to an electrical signal can occur with limited energy loss to heat [5, 6].

A few challenges are encountered in the area of piezoelectric transducers for energy conversion. By far, the most applied and highest performing materials are based on $Pb(Zr,Ti)O_3$ and contain a significant amount of lead oxide, toxic to humans and the environment [7–10]. With the prospect of the widespread use of piezoelectrics as energy harvesters for consumer wearables, internet-of-things devices etc, with low anticipated rate of recycling and proper disposal, the use of lead-containing materials is especially critical. The use of lead oxides in consumer electronics is also addressed in upcoming legislation e.g. in the European Union [11].

However, lead-free alternatives generally suffer from lower performance than those that are lead-based [9]. The drop in performance can to some extent be overcome by materials engineering, e.g. alignment of the crystallographic directions of the grains in the ceramics (texturing) [12–14], such that the direction of largest piezoelectric response is utilized [15, 16]. For bulk materials, texturing does however require several extra, cumbersome processing steps compared to simple pressing and sintering of powder. The processing must now introduce shear forces (e.g. via tape casting) that align template particles and thereby steer the growth into the desired crystallographic direction (templated grain growth) [13], followed by the lamination of many thin layers to form the desired bulk material thickness. For certain systems, such as energy harvesters [3, 17, 18], large-scale structural health monitoring [19], high-frequency ultrasound transducers [5, 20], large area and low dimensionality in the form of a thick film (1–100 μm thickness) is the desired shape rather than bulk. For these shapes, the more complex geometry already requires complex shaping, and achieving texture should only require the addition of template particles for texture development. However, thick films have limited strength and are usually not self-supporting, such that a support layer (substrate) is required. So far, the co-sintering of textured piezoelectric thick films and supports have not been realized.

This work therefore develops the synthesis of, and investigates energy conversion in this new type of textured, multilayer piezoelectric transducers made by tape casting. The motivation behind this, is that tape casting makes it possible to induce texture in the thick film by adding templates that steer the direction of grain growth [13]. Furthermore, porosity can be introduced by adding pore formers [21], such that porous backing layers can be made to adjust the density, acoustic impedance and attenuation of sound waves, important for applications in ultrasound transducers. Several layers of tape can be laminated (or potentially co-cast) to the desired layer configuration or to increase the thickness. Co-sintering this entire structure could make it possible to avoid weak interfaces and limited temperature stability from gluing layers together after sintering. The glue layers (typically epoxy resins) can significantly modify the behavior of the device, in particular the electroacoustic response of an ultrasound transducer if the thickness of this layer is in the same order of magnitude as the thickness of the thick film [22].

This work shows how such textured, multilayered transducers can be synthesized and how the texture affects the energy conversion between the electric and mechanical domain and the physical properties of the transducers. The test material is the lead-free piezoelectric composition $Li_{0.06}(K_{0.52}Na_{0.48})_{0.94}Nb_{0.71}Ta_{0.29}O_3$ with 0.25 mol% Mn (KNNLTM). This is a modified version of the promising lead-free system based on $K_{0.5}Na_{0.5}NbO_3$ (KNN) [9, 23, 24]. The specific KNNLTM composition was recently found to have large coupling coefficients for mechanical-electrical energy transfer when made as (100)-oriented single crystals [25]. We observe that a high degree of texture can be obtained in KNNLTM thick films co-sintered on a porous KNNTLM support after careful process control. Four multilayered, co-sintered samples are characterized in detail in this work, two textured and two non-textured, showing the highest piezoelectric response in the most textured sample. Although the coupling coefficient between the mechanical and electrical energy in these first samples is low, this work shows the potential for introducing texture in co-sintered multilayered piezoelectric transducers.

Methods

Multilayer transducer fabrication

Slurries for tape casting were produced following a procedure by Foghmoes *et al* [26]. Powder of KNNLTM ($[Li_{0.06}(K_{0.52}Na_{0.48})_{0.94}](Nb_{0.71}Ta_{0.29})O_3$ doped with 0.25 mol% Mn) (Cerpotech A/S, Norway) were mixed with ethanol as solvent, polyvinylpyrrolidone (PVP) (Sigma Aldrich, Germany) as a dispersant and milled for 72 h. A binder system (a mixture of a polyvinyl butyral (PVB) binder (Sekisui Chemical Ltd, USA) and Pycal 94 plasticizer (Tapecasting Warehouse Inc., USA)) [26] was added and the slurry was rolled carefully for 16–24 h before filtering, evacuation and tape casting. To introduce texture, platelet-shaped (100)-oriented $NaNbO_3$ (made in-house according to [27]) corresponding to 10 vol% of the KNNLTM was added to the slurry after filtering, and homogenized by 10 min mixing with a magnetic stirrer and 10 min of ultrasonication before evacuation and tape casting. For the slurries for the porous support, 50 vol% of the KNNLTM was replaced by polymethyl methacrylate (PMMA) (type 10G (d_{50} of 9 μm), Esprix, USA) or graphite (type UF1 (d_{50} of 3 μm), Graphit Kropfmühl AG, Germany) as pore formers [28–30]. The pore formers were added together with the KNNLTM powder at the start of the process. The tape casting speed was 20 cm min^{-1} for all tapes. Dense layer tapes were cast with a doctor blade gap of 200–400 μm, porous layer tapes 500–1000 μm and air-dried overnight. Dried tape cast sheets were screen printed with Pt paste (product #5542, ESL ElectroScience, PA, USA) and laminated at 110 °C while the electrode paste was wet. Debinding and sintering were performed in air with the samples kept flat by two alumina plates. The thermal program was: heating with 15 °C h^{-1} to 200 °C (isothermal hold for 2 h), 6 °C h^{-1} to 300 °C (isothermal hold for 2 h), 6 °C h^{-1} to 350 °C (isothermal hold for 2 h),

6 °C h^{-1} to 410 °C (isothermal hold for 2 h), 6 °C h^{-1} to 450 °C (isothermal hold for 2 h), 15 °C h^{-1} to 600 °C (isothermal hold for 4 h), 200 °C h^{-1} to 1100 °C (isothermal hold for 14 h), cooling with 200 °C h^{-1} to 25 °C.

Characterization

Debinding and densification of the tapes were studied with thermogravimetric analysis (TGA) and differential thermal analysis (DTA) (STA 409PC/PG, Netzsch, Germany), contact dilatometry (DIL 402, Netzsch, Germany) and optical dilatometry (TOMMI, Fraunhofer Institut für Silicatforschung ISC, Würzburg, Germany). Scanning electron microscopy (SEM) was conducted with a Hitachi TM3000 (Hitachi High-Technologies Europe GmbH, Germany) to investigate the microstructure of the sintered multilayers. The samples were mounted in epoxy with the cross-section up and polished with a 0.25 μm diamond suspension before SEM. The software ImageJ (version 1.48v, Wayne Rasband, National Institute of Health, USA) was used to analyze the porosity in the multilayers from the micrographs of their cross-sections. X-ray diffraction (XRD) was conducted on as-sintered top surfaces of the multilayers with a Bruker D8 (Bruker, USA) to investigate the structure, phase purity and texture. Texture was calculated based on the intensity of the $\{h00\}$ reflections relative to the other reflections according to the Lotgering equation [31].

The sintered multilayer samples were contacted by Ag paste (product AGG3790, Agar Scientific, UK) painted as one electrode on the top, and one electrode on the side in contact with the middle, co-sintered Pt electrode. Four co-sintered, multilayered samples were characterized in detail, two textured and two non-textured. Ferroelectric response was measured with a TF2000 ferroelectric characterization system (aixACCT, Germany), then samples were poled at 3 kV mm^{-1} for 30 min at room temperature. The electromechanical thickness mode properties of the thick films were deduced from the measurements with a spectrum analyzer (Agilent 4395 A, Palo Alto, CA, USA) of the complex electrical impedance as a function of frequency. The one-dimensional KLM equivalent electrical circuit [32–34] was used to calculate the theoretical behavior of the electrical impedance of the multilayer structure. From the experimental data, a fitting process was implemented to deduce several thickness mode parameters of the piezoelectric thick films [22, 35] The studied structures are composed of four layers with porous substrate, bottom Pt and top Ag electrodes and the piezoelectric thick film. Parameters of the electrodes were taken from Selfridge [36] and acoustic parameters of the porous substrate were measured with two ultrasound transducers according to the procedure described in Bakarič *et al* [37]. All the physical and dimensional properties of the three inert layers were considered as constant, along with thickness and density of the thick films in the KLM model. Finally, five thickness mode parameters of the thick films were deduced: the longitudinal wave velocity C_L, the dielectric constant at constant strain $\varepsilon_{33}{}^S/\varepsilon_0$, the effective thickness coupling factor k_t and the loss factors (mechanical: tan δ_m, electrical: tan δ_e).

Results

Fabrication of slurries, tapes and multilayers

The results of the thermal analysis (TGA and DTA) are shown in figure 1. The dense tape contains no pore former and therefore has the lowest mass loss (35 wt%). Its mass loss occurs gradually from 100 °C to 400 °C, with a marked exothermic DTA signal around 400 °C from the binder burning out. The tape with graphite as a pore former also shows a similar exothermic reaction, although a little shifted to higher temperatures, followed by another exothermic signal as the graphite starts to burn at around 550 °C. The total mass loss of the graphite-based tape is very high (60 wt%). Using PMMA as a pore former results in an endothermic debinding as the PMMA decomposes around 400 °C, masking the exothermic signal from the binder. This tape has a total weight loss of 50 wt%.

Figure 2 shows the shrinkage and shrinkage rate of the tapes during debinding and sintering, measured with both contact and optical dilatometry. In the contact dilatometer (figure 2(a)) all samples shrink significantly already at 50 °C–150 °C, then more at 700 °C. The dense tape shows a further shrinkage at 1100 °C. The second shrinkage step, around 700 °C, is a little delayed in the PMMA-based tape compared to the dense tape, and spans over a wider temperature range in the graphite-based tape (easiest to observe from the shrinkage rates in figure 2(b)). The final shrinkage around 1100 °C is also less pronounced in these two tapes with pore formers than the dense tape. All samples have a high total shrinkage: 39% in the dense tape, 66% in the PMMA tape and 79% in the graphite tape. The largest factor in these different total shrinkages is the extent of shrinkage at low temperature (50 °C–150 °C), which is strongly enhanced in the tapes with pore former tapes compared to the dense tape. Shrinkage at such low temperatures cannot occur due to densification, but can be an effect of the load from the contact dilatometer pushrod on the soft tapes. Measurements with an optical dilatometer (only available up to 1000 °C) were therefore performed to avoid the samples being mechanically deformed. Here, we see that the overall shrinkage is lower, and especially the significant shrinkage at low temperatures is avoided

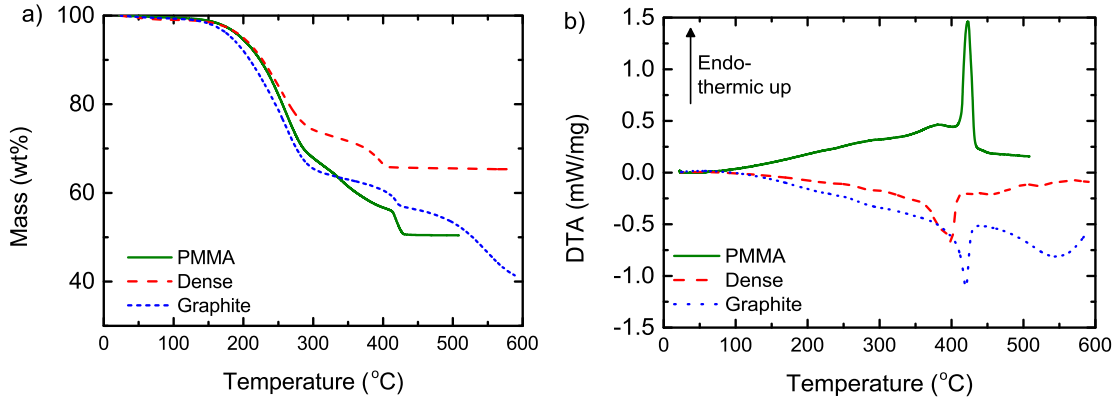

Figure 1. (a) TGA and (b) DTA signal of the tapes for dense KNNLTM or porous KNNLTM (either graphite or PMMA added as pore formers).

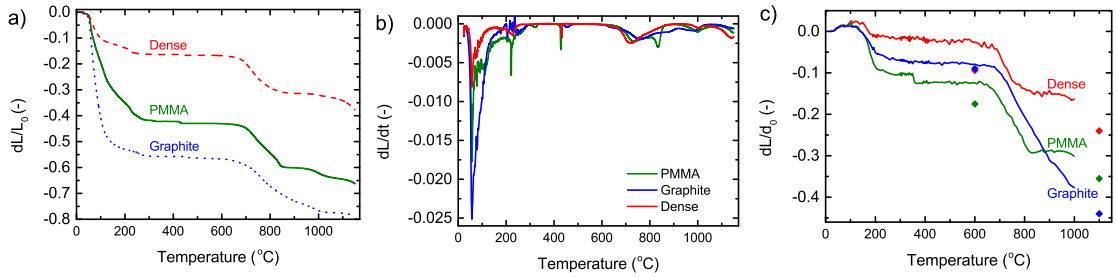

Figure 2. Shrinkage and shrinkage rate of tapes rolled into cylinders, measured by dilatometry. (a), (b) Contact dilatometry and (c) optical dilatometry. The extra data points in (c) are shrinkage measured from dimensions of actual samples after debinding and sintering steps performed in the furnace.

(figure 2(c)). Still, the overall order of total shrinkage is the same as for the measurements with the contact dilatometer. The shrinkage observed with real samples after the debinding part only, and after the complete debinding and sintering program (see Methods section) are in good agreement with the predictions from the optical dilatometer.

Microstructures of co-sintered transducers of dense layers on porous supports are shown in figure 3. Please note that the right hand side column is a higher magnification version of the image in the left hand side column. Figure 3(a) shows the textured, dense layer on the PMMA-based porous support. From the top to the bottom in this micrograph is the outer Ag electrode, the thick KNNLTM film, the inner Pt electrode and the porous KNNLTM substrate. The outer Ag electrode (applied after sintering to avoid diffusion into the KNNLTM) is 10–20 μm thick, quite porous (55%–75% dense) and adheres well to the dense KNNLTM layer. The textured KNNLTM layer is 50–75 μm thick, 81%–86% dense and has some distinct, large (~10 μm) brick-shaped grains from the templated grain growth process. The Pt electrode is close to 100% dense and ~5 μm thick, with a few discontinuities in the shown 2D section of the sample. The adherence between the KNNLTM dense tape and the inner Pt electrode is very good, while in samples made on very thick supports (985 μm, not shown), a tiny gap (<1 μm) between the KNNLTM dense tape and the Pt could be observed. Laminating samples after the Pt electrode had dried caused a macroscopically visible delamination in all samples (not shown). The microstructure of the PMMA-based porous support contains the typical cube grains (<10 μm) of KNN-based piezoelectrics, with some irregular, spherical pores (~10 μm) after pyrolysis of the PMMA spheres. The porous PMMA-based support has a density of around 55%. Figure 3(b) shows a sample of the same layer configuration as (a), but without texture in the dense layer. The overall structure is similar, but the dense KNNTLM layer is denser (92%). Initial studies with co-sintering the dense KNNLTM tapes with porous tapes made with graphite as the pore former resulted in completely delaminated and curled porous tape, as seen in figure 4(a). From the microstructure image in figure 3(c)) (only graphite-based layer visible), we can also see that the graphite pore former resulted in less pronounced pore morphology, smaller pores (<5 μm) and very low porosity (83% dense). PMMA-based tapes were therefore chosen as the porous support for the remainder of this study, due to

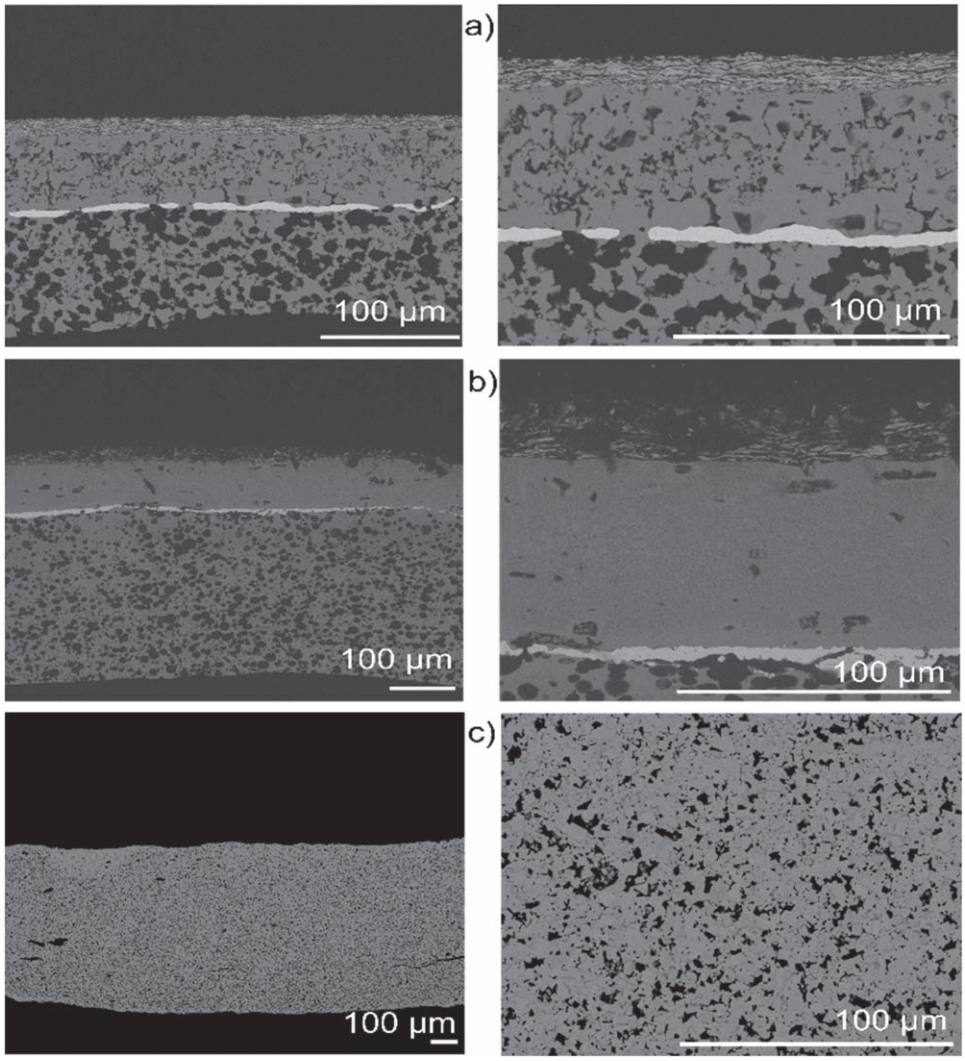

Figure 3. Microstructure of sintered KNNLTM. (a) textured, dense layer on porous PMMA-based support (sample 1-textured), (b) non-textured layer on porous PMMA-based support (sample 3-non-textured), (c) porous graphite-based support. The pictures on the right hand side are all higher magnification of the sample on the left hand side.

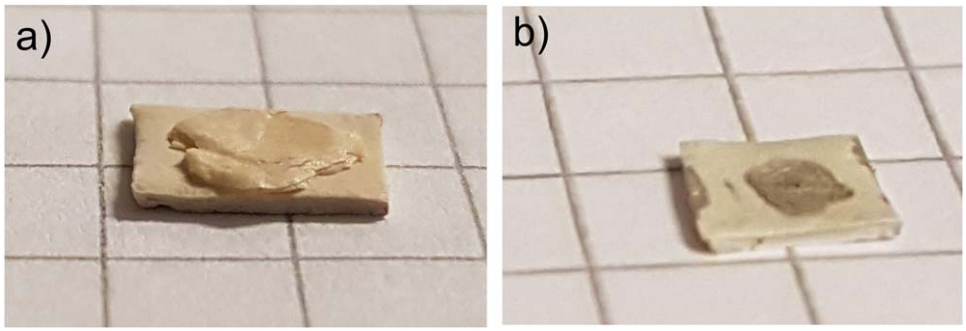

Figure 4. (a) Picture of attempted co-sintering of porous tape with graphite as pore former (top layer) with dense KNNTLM layer (bottom part). (b) Successfully co-sintered sample PMMA as pore former (bottom layer) with dense KNNLTM (top layer), and contacting for characterization with silver in painted as top electrode (darker circle) and on sides to contact the inner Pt electrode. Each sample is pictured on a paper with 5 × 5 mm squares.

their higher porosity and compatibility in co-sintering. An example of a successful co-sintering and contacting for electromechanical testing is shown in figure 4(b).

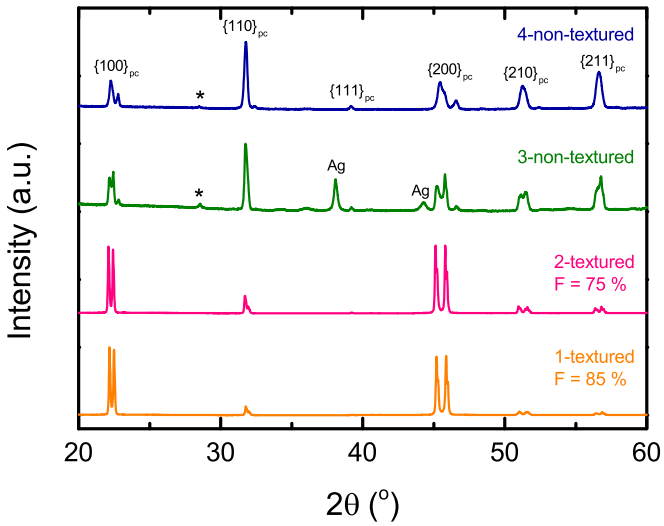

Figure 5. XRD patterns of the top of the co-sintered KNNLTM multilayer transducers. The patterns are indexed with KNNLTM peaks according to PDF 32-0822 for $KNbO_3$ (isostructural to KNNLTM) and JCPDS 04-0783 for Ag. Possible Nb-rich secondary phases are marked with *.

Table 1. Properties of KNNLTM multilayer transducers.

Sample		1-textured	2-textured	3-non-textured	4-non-textured
Dense layer rel. density	(%)	81	84	92	95
Dense layer texture	(%)	85	75	—	—
Dense layer thickness	(μm)	49	84	73	86
Support thickness	(μm)	86	435	239	238
Support rel. density	(%)	54	60	61	61
P_r	(μC cm^{-2})	5.7	8.0	8.4	19.9
E_c	(kV mm^{-1})	0.8	1.4	1.3	1.7
k_t	(%)	18	11	14	9
$\varepsilon_{33}{}^S/\varepsilon_0$	(-)	245	205	430	240
$C_{33}{}^D$	(GPa)	63.3	65.1	95.3	74.3
C_L	(m s^{-1})	3900	3900	4500	3915
Z_{ac}	(MRayl)	16	17	21	19

Characterization of co-sintered multilayers

Figure 5 shows the XRD patterns of co-sintered KNNLTM multilayer transducers recorded from the sample top surface. Some peaks from parts of the Ag electrode are visible in one of the samples at 38° and 44° 2θ. The main phase of all samples is KNNLTM. Some reflections between 20° and 30° 2θ are visible to various extents, typical for Nb-rich secondary phases (e.g. $K_2Nb_4O_{11}$ or K_4Nb_6O17) [38, 39]. The largest differences between the samples are the relative intensities of the KNNLTM reflections. An increase in the {h00} type reflections versus the other {hkl} indicates that the desired (100)-type texture has been successfully introduced in the sample (the quantified volume of texture given by the Lotgering calculation is shown in the figure).

The results of the electromechanical performance are summarized in table 1 at the end of this section. When analyzing the properties, it should be kept in mind that the non-textured samples have significantly higher density (92%–95%) than the textured samples (81%–84%), as can be seen in figure 6. The ferroelectric response of the multilayers is shown in figure 7. From the hysteresis loops in figure 7(a), we can see that the polarization-electric field response of the samples shows ferroelectric hysteresis. The magnitudes of the saturated (P_s) and remanent (P_r) polarization, the coercive field (E_c) and the gap between the start and end polarization values differ strongly between the samples. For example, P_r varies from 6 to 20 μC cm^{-2}, which is in the typical range for KNN-based samples [8] while the specific KNNTLM composition is expected to have ~17 μC cm^{-2} in non-textured KNNLTM [40], and ~7 μC cm^{-2} in (100)-oriented single crystal KNNLTM [25]. The polarization decreases in the textured compared to non-textured samples, expected from both due to the alignment of the polar axis off the direction of the electric field and the lower density in these samples compared to the non-textured [41]. Unexpected high polarization response is a typical sign of leakage current, contributions to the polarization signal [41]. From the current signal in figure 7(b) it is easier to distinguish the contribution of

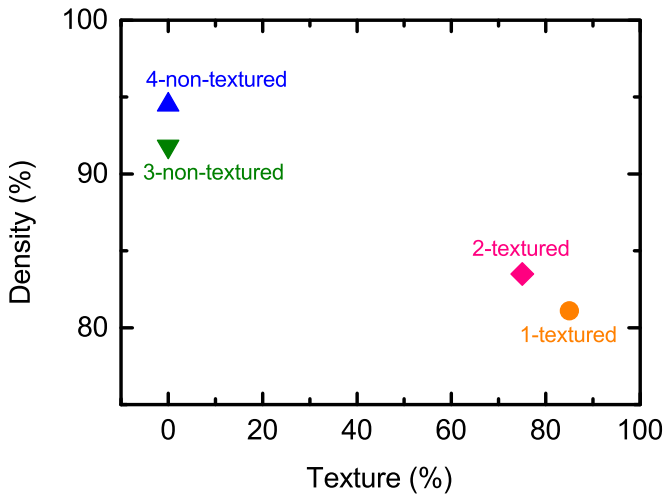

Figure 6. Density versus texture of the KNNLTM dense layer of the multilayer structures.

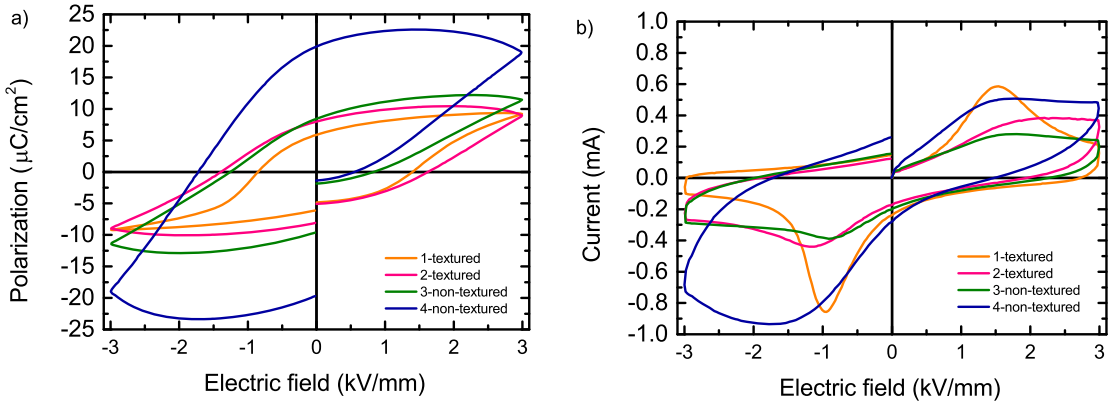

Figure 7. Ferroelectric response of the KNNLTM multilayer transducers. (a) Polarization versus electric field loops measured at 100 Hz and 3 kV mm^{-1}. (b) Corresponding current signal.

leakage current and ferroelectric switching current, as the latter is a peak occurring at the coercive field, while the former occurs at all field strengths, sometimes increasing with the field strength magnitude. All samples display signs of ferroelectric switching, but it is obvious that sample 4-non-textured is dominated by leakage current rather than switching current. We can also observe a strong asymmetry between the positive and negative field direction, which is common for systems of asymmetric samples and electrode configuration, like the different top and bottom electrodes used in this work [41].

The real and imaginary parts of the electrical impedance (Z), recorded from the poled samples and fitted to the KLM model, are shown in figure 8 (for two samples). The thickness of the porous substrate was in the same range as the ratio of longitudinal wave velocity in this substrate to the fundamental resonance frequency of the piezoelectric thick film (in free resonator conditions), which leads to several peaks (coupled resonance) [42]. Moreover, the bottom platinum electrode must be taken into account since the thickness is also of the same order as the piezoelectric thick films.

The results from the KLM model applied to the impedance spectra are shown in figure 9 as a function of the degree of texture in the samples. The dielectric constant at constant strain (figure 9(a)) is around 200–400 for non-textured samples, and decreases to 250 in the textured samples. This is in agreement with both their higher porosity and previous studies on textured KNN-based samples [43]. The elastic constant $C_{33}{}^{D}$ (figure 9(b)), deduced from the longitudinal wave velocity and density, is decreasing with texture, probably related to their higher porosity compared to the non-textured samples. Figure 9(c) shows the thickness coupling coefficient, k_t, of the samples. Here, we can see that the highest k_t value (18%) is in the sample with the highest degree of (100) texture. The KLM model also gives values for the mechanical and dielectric loss, but both the values of the mechanical losses (20%–30%) and the electrical loss values (2.2%–3.7%) are unreliably high in our materials, probably related to inhomogeneous thickness that the 1D model cannot account for. The acoustic impedance,

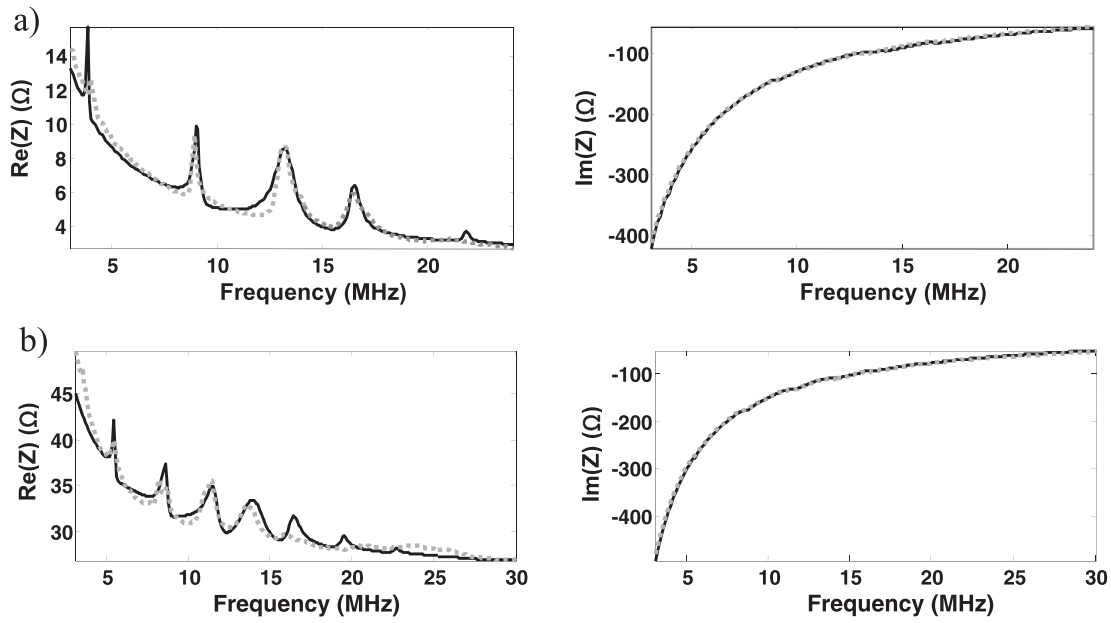

Figure 8. Electrical impedances of the KNNLTM multilayer structures. (a) 2-textured, (b) 4-non-textured. The measured impedances are shown with gray, dashed lines, the fit to the KLM model with black solid lines.

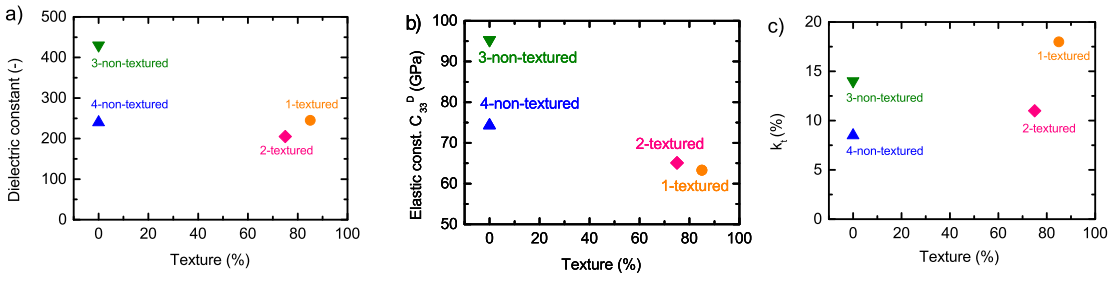

Figure 9. Physical parameters derived from the KLM analysis of the impedance spectra of the KNNLTM multilayer transducers. (a) Dielectric constant at constant strain, $\varepsilon_{33}{}^{S}/\varepsilon_0$, (b) elastic constant, $C_{33}{}^{D}$, and (c) thickness coupling coefficient, k_t.

Z_{ac}, of the samples can be calculated from the longitudinal wave velocity, C_L, from the KLM model combined with the density, ρ, from $Z_{ac} = \rho C_L$. The acoustic impedance of the multilayer samples is in the range of 16–21 MRayl (table 1).

Discussion

Fabrication of multilayered KNNLTM transducers

The thermal analysis shows several aspects that need to be considered for successful multilayer fabrication. TGA results (figure 1(a)) show that the co-sintering, especially the porous part, requires careful control of the thermal program and access to air, such that the debinding and mass loss can occur without damaging the samples. This was successfully achieved with the debinding program presented in the Methods section with isothermal holds, where the mass loss is strongest, and the use of a furnace with flowing air. The flowing air is especially crucial since the samples had to be kept between alumina plates to stay flat. Differences in sintering shrinkage is also a potential cause of bending and delaminations during sintering [44], which is observed to some extent by the slight curvature of the multilayers (direction of bending agrees with a higher shrinkage of the porous layer versus the dense, figure 3). The overall shape of the tapes' dilatometry curves resemble that of powder of the same composition [40], but the differences in the magnitude of shrinkage is related to the softness and compressibility at low temperature, and extra shrinkage related to the use of pore formers [21]. Here, the choice of PMMA as the pore former made it possible to limit the differences in total shrinkage to ~10% between the dense and the porous layers, and successfully co-sinter this combination, in contrast to the delamination seen with graphite (20% shrinkage difference) (figures 3(c) and 4(a)). Since the dense and the porous layers are both KNNLTM, no

cracking or delamination due to differences in thermal expansion coefficients (TEC) are expected. Although the TEC of Pt is quite low (~9 * 10^{-6} K^{-1}) [45] compared to other metals, the difference from the TEC of KNNLTM is probably more than 1 * 10^{-6} K^{-1} (the TEC of KNN is ~7 * 10^{-6} K^{-1}) [46]. In our system, the stresses due to sintering or TEC mismatches might be somewhat alleviated by the porosity (decreasing stiffness and thus increasing crack resistance) [47] and the low layer thickness (decreasing the total energy) of the Pt layer [48]. Still, the TEC mismatch or sintering stress could be the origin of the minor delaminations between Pt and KNNLTM observed if the support layer thickness was increased.

Densification of KNN-based ceramics is generally challenging [40, 49], which is also reflected in the density of the textured multilayer transducers made in this work. A density of 81%–84% in the textured layers is significantly lower compared to what can be expected in bulk ceramics [24, 40]. Low density is known to cause a reduction of the dielectric permittivity and piezoelectric coefficients such as d_{33} in the transducers, but does not have such a strong effect on the k_t coupling coefficient [50]. In the non-textured samples, the density is higher, implying that the templated grain growth into texture hinders the densification. Combined with the development of a sufficient degree of texture in the thick films, without any limitations in the support thickness, these are important contributions to the research on textured ceramics. First of all, it challenges the conception that templated grain growth only occurs at >95% density [51]. Secondly, it demonstrates that templated grain growth also can occur in thick films, where the feature size is lower than in bulk samples, and also when co-sintered in a multilayered structure. This is promising for the introduction of texture in other novel geometries with fine feature size, such as 3D printed structures.

Electromechanical performance of the multilayered KNNLTM transducers

The results from the KLM model based on the electrical impedance measurements show that the texture, as expected, improves the piezoelectricity, in the form of the thickness coupling coefficient k_t. Due to the manufacturing technique (several manual process steps and thin layers), a higher sample-to-sample variation can be expected for thick film multilayered samples, compared to bulk samples made by pressing powders and sintering pellets followed by machining and polishing surfaces. We do observe some variations in performance between otherwise similar samples (3-non-textured and 4-non-textured) especially in the dielectric permittivity and coupling coefficient (figure 9). Despite the higher density in 4-non-textured, this sample has lower dielectric permittivity than 3-non-textured. When evaluating the ferroelectric response, it is obvious that sample 4-non-textured has a higher conductivity than 3-non-textured (figure 7). This could indicate chemical impurities, secondary phases, variations in thickness and electrode coverage, or other microstructural features that promote lower dielectric permittivity and pathways of higher conductivity throughout the thick film. The small differences between samples 1-textured and 2-non-textured can be ascribed to the small difference in the degree of texture, but also here, microstructural or chemical effects could come into play. Still, such defects are expected to be possible to limit if the multilayered synthesis is carefully controlled, as all the techniques utilized (with the exemption of the synthesis of $NaNbO_3$ particles for templated grain growth) are up-scalable and shown to be ideal for fabrication of e.g. multilayered ceramic capacitors [52] once transferred to industrial environments. This is not the scope of this study, but rather it demonstrates that the introduction of texture increases the performance for energy conversion, and that tape casting and co-sintering of multilayers with textured piezoelectrics are possible.

As a lead-free material system, the KNNLTM multilayers have an advantage for energy harvesting for consumer electronics. The most promising application would be as large-area harvesters at elevated temperature, in order to best utilize the scalability of the processing techniques applied and the higher temperature stability of the co-sintered system compared to glued transducers, which can mechanically deform above 70 °C. The low mechanical quality factor corresponds to a large frequency bandwidth, advantageous for energy harvesting from environments with a large variation in vibration sources [3]. The low permittivity is also an advantage for use in a non-resonant application, where $d_{ij}^2/\varepsilon_{ii,r}$ is the figure of merit [9]. Still, the low value of the k_t is usually connected with a low transverse coupling coefficient, k_{31}, and transverse piezoelectric charge coefficient d_{31}, important for energy harvesting in a cantilever structure. Higher coupling coefficients and charge coefficients could potentially be obtained by optimizing the poling parameters, for example by increasing time, electric field strength, and especially the temperature during poling. Furthermore, increasing the density of the dense layer could be very important for an energy harvester operating at resonance, where the figure of merit is k^2 * Q_m ($Q_m = 1/\tan\delta_m$) [3]. Since a denser material has lower mechanical losses (because porosity increases acoustic attenuation, which is related to mechanical losses in piezoelectric material), denser materials should have a higher figure of merit at resonance frequency. Improving the density would require careful optimization of all processing steps, from powder preparation to a sintering program.

As thick films supported on porous substrates, these transducers have many advantages for use in high-frequency medical ultrasounds. The low acoustic impedance (<20 MRayl) compared to the traditional lead-based systems (>30 MRayl) [53] are very favorable, since an impedance value closer to that of biological tissue

(1.5 MRayl) [53] reduces the loss of ultrasonic energy across the interfaces between the transducer and the biological tissue to be examined. The relatively low dielectric permittivity of the transducers and the values of the sound velocity are suitable for a single-element transducer operating at high-frequency [9]. Still, the thickness coupling coefficient should be increased to values above 30%. Improving the poling conditions, as discussed above, is the best pathway towards this. The substrate layer should also be thicker or more porous, such that the coupled resonator behavior is suppressed, and this layer can be considered as a backing with a semi-infinite medium behavior. The co-sintering process has the advantage of producing layers of similar acoustic impedance compared to gluing the piezoelectric to a backing, typically with a low acoustic impedance polymer-based glue [22]. In general, the integrated, co-sintered multilayer structure with texture demonstrated for the first time in this work has, once slightly higher coupling coefficients are realized, promise for use in ultrasound transduction.

Conclusion

Piezoelectric transducers of the lead-free composition $Li_{0.06}(K_{0.52}Na_{0.48})_{0.94}Nb_{0.71}Ta_{0.29}O_3$ with 0.25 mol% Mn (KNNLTM) were studied as multilayers made by tape casting and co-sintering. By using PMMA as the pore former, porous support layers could successfully be co-sintered with a dense KNNLTM thick film and Pt inner electrode, while tapes with graphite as the pore former could not be co-sintered due to larger differences in shrinkage. Texture up to 85% in the [100] crystallographic direction could be developed by templated grain growth from $NaNbO_3$ templates. This sample with the highest degree of texture, displayed the highest piezoelectric response in form of the highest thickness coupling coefficient k_t of 0.18. Our work demonstrates that introduction of texture and increased piezoelectric response is possible via co-sintering on porous substrates, and that this method has promise for applications for ultrasound transducers and energy harvesting.

Acknowledgments

A B H would like to thank Søren Christensen and Dr Kjeld Bøhm Andersen for assistance with tape casting, Ebtisam Abdellahi for assistance with sample preparation for SEM, and funding from Independent Research Fund Denmark, grant DFF-6111-00440, Siemensfonden and Brødrene Hartmanns Fond.

ORCID iDs

Astri Bjørnetun Haugen https://orcid.org/0000-0001-6981-9856
Erling Ringgaard https://orcid.org/0000-0002-0418-9053

References

[1] Jaffe B, Cook W and Jaffe H 1971 *Piezoelectric Ceramics* (New York: Academic)
[2] Haertling G H 1999 Ferroelectric ceramics: history and technology *J. Am. Ceram. Soc.* **82** 797
[3] Priya S 2007 Advances in energy harvesting using low profile piezoelectric transducers *J. Electroceramics* **19** 165–82
[4] Sodano H A, Park G, Leo D J and Inman D J 2003 Use of piezoelectric energy harvesting devices for charging batteries *Proc. SPIE* **5050** 101–8
[5] Shrout T R 2008 Innovations in piezoelectric materials for ultrasound transducers *2008 17th IEEE Int. Symp. Appl. Ferroelectr. (Piscataway, NJ)* (IEEE) pp 1–4
[6] Szabo T L 2014 *Diagnostic Ultrasound Imaging: Inside Out* (Amsterdam: Elsevier) (https://doi.org/10.1016/C2011-0-07261-7)
[7] Flora G, Gupta D and Tiwari A 2012 Toxicity of lead: a review with recent updates *Interdiscip. Toxicol.* **5** 47–58
[8] Rödel J, Jo W, Seifert K T P, Anton E M, Granzow T and Damjanovic D 2009 Perspective on the development of lead-free piezoceramics *J. Am. Ceram. Soc.* **92** 1153–77
[9] Rödel J, Webber K G, Dittmer R, Jo W, Kimura M and Damjanovic D 2015 Transferring lead-free piezoelectric ceramics into application *J. Eur. Ceram. Soc.* **35** 1659–81
[10] Shrout T R and Zhang S J 2007 Lead-free piezoelectric ceramics: alternatives for PZT? *J. Electroceramics* **19** 111–24
[11] European Parliament and The Council Of The European Union 2003 EU-Directive 2002/96/EC: waste electrical and electronic equipment (WEEE) *Off. J. Eur. Union* **46** 24–38
[12] Saito Y, Takao H, Tani T, Nonoyama T, Takatori K, Homma T, Nagaya T and Nakamura M 2004 Lead-free piezoceramics *Nature* **432** 1–4
[13] Messing G *et al* 2004 Templated grain growth of textured piezoelectric ceramics *Crit. Rev. Solid State Mater. Sci.* **29** 45–96
[14] Grivel J C, Thydén K, Bowen J R and Haugen A B 2018 Deposition of highly oriented (K,Na)NbO_3 films on flexible metal substrates *Thin Solid Films* **650** 7–10
[15] Haugen A B, Morozov M I, Johnsson M, Grande T and Einarsrud M-A 2014 Effect of crystallographic orientation in textured $Ba_{0.92}Ca_{0.08}TiO_3$ piezoelectric ceramics *J. Appl. Phys.* **116** 134102
[16] Damjanovic D, Budimir M, Davis M and Setter N 2007 Piezoelectric anisotropy: enhanced piezoelectric response along nonpolar directions in perovskite crystals *Front. Ferroelectr. A Spec. Issue J. Mater. Sci.* **1** 65–76
[17] Li H, Tian C and Deng Z D 2014 Energy harvesting from low frequency applications using piezoelectric materials *Appl. Phys. Rev.* **1** 041301

[18] Toprak A and Tigli O 2014 Piezoelectric energy harvesting: state-of-the-art and challenges *Appl. Phys. Rev.* **1** 031104
[19] Sodano H A, Park G and Inman D J 2004 An investigation into the performance of macro-fiber composites for sensing and structural vibration applications *Mech. Syst. Signal Process.* **18** 683–97
[20] Kuscer D, Abelard A P, Kosec M and Levassort F 2013 Piezoelectric thick-film structures for high-frequency applications prepared by electrophoretic deposition *Ceram. Trans.* **240** 131–41
[21] Corbin S F and Apté P S 1999 Engineered porosity via tape casting, lamination and the percolation of pyrolyzable particulates *J. Am. Ceram. Soc.* **82** 1693–701
[22] Marechal P, Levassort F, Holc J, Tran-Huu-Hue L-P, Kosec M and Lethiecq M 2006 High-frequency transducers based on integrated piezoelectric thick films for medical imaging *IEEE Trans. Ultrason. Ferroelectr. Freq. Control* **53** 1524–33
[23] Rödel J and Li J-F 2018 Lead-free piezoceramics: status and perspectives *MRS Bull.* **43** 576–80
[24] Malič B, Benčan A, Rojac T and Kosec M 2008 Lead-free piezoelectrics based on alkaline niobates: synthesis, sintering and microstructure *Acta Chim. Slov.* **55** 719–26
[25] Huo X *et al* 2015 (K,Na,Li)(Nb,Ta)O_3:Mn lead-free single crystal with high piezoelectric properties *J. Am. Ceram. Soc.* **98** 1829–35
[26] Foghmoes S, Teocoli F, Brodersen K, Klemensø T and Della Negra M 2016 Novel ceramic processing method for substitution of toxic plasticizers *J. Eur. Ceram. Soc.* **36** 3441–9
[27] Chang Y, Yang Z, Chao X, Liu Z and Wang Z 2008 Synthesis and morphology of anisotropic $NaNbO_3$ seed crystals *Mater. Chem. Phys.* **111** 195–200
[28] Haugen A B, Geffroy A, Kaiser A and Gil V 2018 MgO as a non-pyrolyzable pore former in porous membrane supports *J. Eur. Ceram. Soc.* **38** 3279–85
[29] Haugen A B, Gurauskis J, Kaiser A and Søgaard M 2017 Graphite and PMMA as pore formers for thermoplastic extrusion of porous 3Y-TZP oxygen transport membrane supports *J. Eur. Ceram. Soc.* **37** 1039–47
[30] Schmidt C G, Andersen K B, Fu Z, Hansen K K, Roosen A and Kaiser A 2015 Effect of pore formers on properties of tape cast porous sheets for electrochemical flue gas purification *J. Eur. Ceram. Soc.* **36** 645–53
[31] Lotgering F K 1960 Topotactical reactions with ferrimagnetic oxides having hexagonal crystal structures—II *J. Inorg. Nucl. Chem.* **16** [1956] 100–8
[32] Krimholtz R, Leedom D A and Matthaei G L 1970 New equivalent circuits for elementary piezoelectric transducers *Electron. Lett* **6** 398
[33] van Kervel S J H and Thijssen J M 1983 A calculation scheme for the optimum design of ultrasonic transducers *Ultrasonics* **21** 134–40
[34] Lethiecq M, Patat F, Pourcelot L and Tran-Huu-Hue L P 1993 Measurement of losses in five piezoelectric ceramics between 2 and 50 MHz *IEEE Trans. Ultrason. Ferroelectr. Freq. Control* **40** 232–7
[35] Bardaine A, Boy P, Belleville P, Acher O and Levassort F 2008 Improvement of composite sol–gel process for manufacturing 40 μm piezoelectric thick films *J. Eur. Ceram. Soc.* **28** 1649–55
[36] Selfridge A R 1985 Approximate material properties in isotropic materials *IEEE Trans. Sonics Ultrason.* **32** 381–94
[37] Bakarič T, Rojac T, Abellard A-P, Malič B, Levassort F and Kuscer D 2016 Effect of pore size and porosity on piezoelectric and acoustic properties of $Pb(Zr_{0.53}Ti_{0.47})O_3$ ceramics *Adv. Appl. Ceram.* **115** 66–71
[38] Acker J, Kungl H and Hoffmann M J 2013 Sintering and microstructure of potassium niobate ceramics with stoichiometric composition and with potassium- or niobium excess *J. Eur. Ceram. Soc.* **33** 2127–39
[39] Madaro F, Sæterli R, Tolchard J R, Einarsrud M-A, Holmestad R and Grande T 2011 Molten salt synthesis of $K_4Nb_6O_{17}$, $K_2Nb_4O_{11}$ and KNb_3O_8 crystals with needle- or plate-like morphology *CrystEngComm* **13** 1304
[40] Haugen A B 2019 Hybrid atmosphere processing of lead-free piezoelectric sodium potassium niobate-based ceramics *Ceramics* **2** 460–71
[41] Jin L, Li F and Zhang S 2014 Decoding the fingerprint of ferroelectric loops: comprehension of the material properties and structures *J. Am. Ceram. Soc.* **97** 1–27
[42] Lukacs M, Olding T, Sayer M, Tasker R and Sherrit S 1999 Thickness mode material constants of a supported piezoelectric film *J. Appl. Phys.* **85** 2835–43
[43] Haugen A B, Morozov M I, Jones J L and Einarsrud M-A 2014 Rayleigh analysis of dielectric properties in textured $K_{0.5}Na_{0.5}NbO_3$ ceramics *J. Appl. Phys.* **116** 214101
[44] Haugen A B, Aguilera L M, Kwok K, Molla T, Andersen K B, Kaiser A, Hendriksen P V and Kiebach R 2018 Exploring the processing of tubular chromite- and zirconia-based oxygen transport membranes *Ceramics* **1** 229–45
[45] Rumble J (ed) 2019 *CRC Handbook of Chemistry and Physics* 100th edn (Boca Raton, FL: CRC Press)
[46] Malič B, Razpotnik H, Koruza J, Kokalj S, Cilenšek J and Kosec M 2011 Linear thermal expansion of lead-free piezoelectric $K_{0.5}Na_{0.5}NbO_3$ ceramics in a wide temperature range *J. Am. Ceram. Soc.* **94** 2273–5
[47] Kwok K, Frandsen H L, Søgaard M and Hendriksen P V 2014 Stress analysis and fail-safe design of bilayered tubular supported ceramic membranes *J. Memb. Sci.* **453** 253–62
[48] Hendriksen P V, Høgsberg J R, Kjeldsen A M, Sørensen B F and Pedersen H G 2008 Failure modes of thin supported membranes *Adv. Solid Oxide Fuel Cells II Ceram. Eng. Sci. Proceedings* ed N P Bansal, A Wereszczak and E Lara-Curzio Vol 27 (New York: Wiley) ch 34 pp 347–60
[49] Malič B, Koruza J, Hreščak J, Bernard J, Wang K, Fisher J G and Benčan A 2015 Sintering of lead-free piezoelectric sodium potassium niobate ceramics *Materials.* **8** 8117–46
[50] Kuscer D, Levassort F, Lethiecq M, Abellard A-P and Kosec M 2011 Lead-zirconate-titanate thick films by electrophoretic deposition for high-frequency ultrasound transducers *J. Am. Ceram. Soc.* **95** 892–900
[51] Messing G L *et al* 2004 Templated grain growth of textured piezoelectric ceramics *Key Eng. Mater.* **29** 45–96
[52] Ming-Jen P and Randall C A 2010 A brief introduction to ceramic capacitors *Electr. Insul. Mag. IEEE* **26** 44–50
[53] Lethiecq M, Levassort F, Certon D and Tran-Huu-Hue L P 2008 Piezoelectric transducer design for medical diagnosis and NDE *Piezoelectric Acoust. Mater. Transducer Appl.* (Boston, MA: Springer) pp 191–215